AIP | Applied Physics Letters

Highly stable thin film transistors using multilayer channel structure

Pradipta K. Nayak, Zhenwei Wang, D. H. Anjum, M. N. Hedhili, and H. N. Alshareef

Citation: Applied Physics Letters **106**, 103505 (2015); doi: 10.1063/1.4914971
View online: http://dx.doi.org/10.1063/1.4914971
View Table of Contents: http://scitation.aip.org/content/aip/journal/apl/106/10?ver=pdfcov
Published by the AIP Publishing

Highly stable thin film transistors using multilayer channel structure

Pradipta K. Nayak, Zhenwei Wang, D. H. Anjum, M. N. Hedhili, and H. N. Alshareef[a)]
Materials Science and Engineering, King Abdullah University of Science and Technology (KAUST), Thuwal 23955-6900, Saudi Arabia

(Received 30 December 2014; accepted 4 March 2015; published online 12 March 2015)

We report highly stable gate-bias stress performance of thin film transistors (TFTs) using zinc oxide (ZnO)/hafnium oxide (HfO_2) multilayer structure as the channel layer. Positive and negative gate-bias stress stability of the TFTs was measured at room temperature and at 60 °C. A tremendous improvement in gate-bias stress stability was obtained in case of the TFT with multiple layers of ZnO embedded between HfO_2 layers compared to the TFT with a single layer of ZnO as the semiconductor. The ultra-thin HfO_2 layers act as passivation layers, which prevent the adsorption of oxygen and water molecules in the ZnO layer and hence significantly improve the gate-bias stress stability of ZnO TFTs. © *2015 AIP Publishing LLC*. [http://dx.doi.org/10.1063/1.4914971]

Zinc oxide (ZnO) based thin film transistors (TFTs) have been studied intensively during the last decade due to their potential use in flat-panel displays.[1] The tunable conductivity of ZnO thin film makes it a very promising candidate for both passive and active electronic applications.[2–4] Although zinc oxide TFTs with good field-effect mobility have been reported using various deposition techniques,[5–10] the stability of ZnO and other oxide-based TFTs under gate-bias stress is a major concern for display applications.[11–14] Further, the increased temperature of display devices due to prolonged use or operation under harsh conditions can significantly shift the threshold voltage of the pixel-TFTs,[14,15] which would affect the performance of the corresponding device. It has been reported that appropriate doping of the semiconductor layer could improve the gate-bias stress stability of oxide based TFTs.[16,17] However, the TFTs in these cases still show significant threshold voltage shift under gate-bias stress, indicating that substantial improvement in TFT stability still needed for the development of higher performance display devices.

In this work, we report highly stable TFTs using a ZnO/hafnium oxide (HfO_2) multilayer structure semiconducting channel layer. It was found that inserting ultra-thin HfO_2 layers between ZnO layers greatly improves the gate-bias stress stability of ZnO TFTs at room temperature (RT) and as well as at 60 °C, making it suitable for harsh application conditions.

Commercial indium tin oxide (ITO) film deposited on glass substrates was used as the gate electrode. Both HfO_2 and ZnO thin films were deposited using a Cambridge Nanotech atomic layer deposition (ALD) system. Tetrakis (dimethylamido)hafnium(IV), diethylzinc and deionized water were used as the precursors. Three different types of channel layer structures, (i) ZnO (160 cycles), hereafter referred as TFT-A, (ii) ZnO (160 cycles)/HfO_2 (5 cycles), hereafter referred as TFT-B, and (iii) ZnO (53 cycles)/HfO_2 (5 cycles)/ZnO (53 cycles)/HfO_2 (5 cycles)/ZnO (54 cycles)/HfO_2 (5 cycles), hereafter referred as TFT-C, were used to fabricate the TFTs investigated in this work. Zinc precursor was un-heated and hafnium precursor was heated to 75 °C during ALD growth process. The substrate temperature during HfO_2 and ZnO deposition was maintained at 160 °C. The channel layers were patterned by photolithography and wet-etching process. Bilayer of Ti (10 nm)/Au (70 nm) source and drain electrodes with channel width (W) and length (L) of 500 and 100 μm, respectively, were deposited by e-beam/thermal evaporation and were patterned by lift-off method. Finally, all the devices were annealed on a hot-plate at 160 °C for 1 h in ambient air atmosphere. Current-voltage characteristics of the TFTs were measured using an Agilent B1500A semiconductor device parameter analyser.

Schematics of the TFTs with three different types of semiconductor layer structures are shown in Figs. 1(a)–1(c). The transfer characteristic curves of the corresponding TFTs

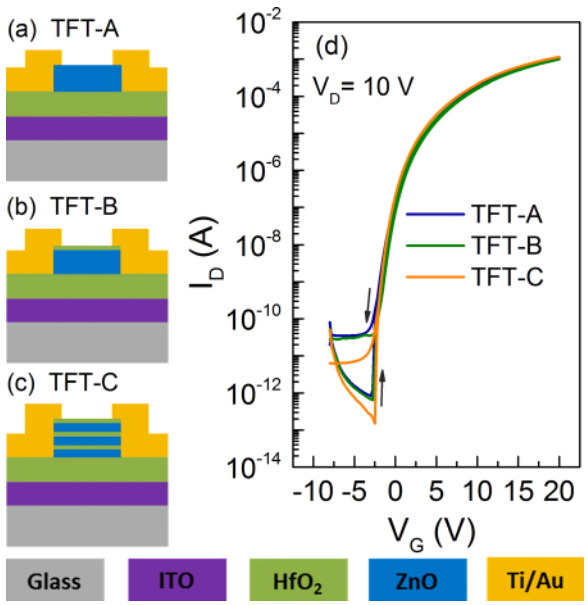

FIG. 1. Schematics of (a) TFT-A, (b) TFT-B, and (c) TFT-C with different types of channel layer structures and (d) transfer characteristics of the corresponding TFTs measured with the forward and backward sweep of gate voltage. The colored rectangles shown in the bottom line represent the different layers used in the schematic TFT structures.

[a)]Author to whom correspondence should be addressed. Electronic mail: husam.alshareef@kaust.edu.sa

are shown in Fig. 1(d). No significant difference in field-effect mobility was observed between the three types of TFTs. The saturation field-effect mobility for the TFT-A, TFT-B, and TFT-C was found to be 13.1, 12.8, and 13.4 $cm^2/V\,s$, respectively. The ratio of the drain on-current to off-current (I_{on}/I_{off}) for the TFT-C ($\sim 8 \times 10^9$) was >7 times higher than that of TFT-A and TFT-B.

Positive gate-bias stress (PBS) and negative gate-bias stress (NBS) measurements were carried out at RT and 60 °C and the results are shown in Figs. 2 and 3. The transfer characteristic curves under PBS and NBS were measured by applying a positive (+10 V) and negative (−10 V) bias, respectively, to the gate terminal. The drain and source voltage during PBS and NBS were fixed as 0 V. Fig. 4 shows the change in threshold voltage and subthreshold swing (*SS*) values for TFT-A and TFT-C measured under PBS and NBS at RT and 60 °C. TFT-A under PBS at RT (Fig. 2(a)) exhibited parallel shifting of the transfer curve in the positive direction with increasing stress duration up to 1000 s with a maximum change in threshold voltage (ΔV_{TH}) of +0.2 V, as shown in Fig. 4(a). No significant change in ΔV_{TH} was observed with further increase in PBS duration. Under PBS at 60 °C (Fig. 2(d)), TFT-A exhibited a higher ΔV_{TH} of +1.3 V after 3000 s compared to the PBS measured at RT, as can be seen from Fig. 4(a). No significant change in subthreshold swing (ΔSS) was observed in case of the PBS measured at RT (Fig. 4(c)), however, ΔSS was increased by 0.03 V/dec in case of the PBS measured at 60 °C. In case of NBS, TFT-A exhibited negative shifting of the transfer characteristic curve with increasing stress duration (Figs. 3(a) and 3(d)). TFT-A under NBS at 60 °C exhibited a very large negative ΔV_{TH} of −2.5 V (after 3000 s) compared to the NBS at RT ($\Delta V_{TH} = -0.6$ V). No significant change in ΔSS was observed in case of NBS measured at RT, however, at 60 °C ΔSS was increased with increasing NBS duration with a maximum of 0.178 V/dec (Fig. 4(c)). TFT-B showed a similar trend of intermediate stability under PBS (Figs. 2(b) and 2(e)) and NBS (Figs. 3(b) and 3(e)). Interestingly, no shifting of the transfer characteristic curve was observed in case of TFT-C under PBS measured at RT (Fig. 2(c)) and as well as at 60 °C (Fig. 2(f)). Further, TFT-C showed very stable transfer characteristic curves under NBS at RT (Fig. 3(c)) with no

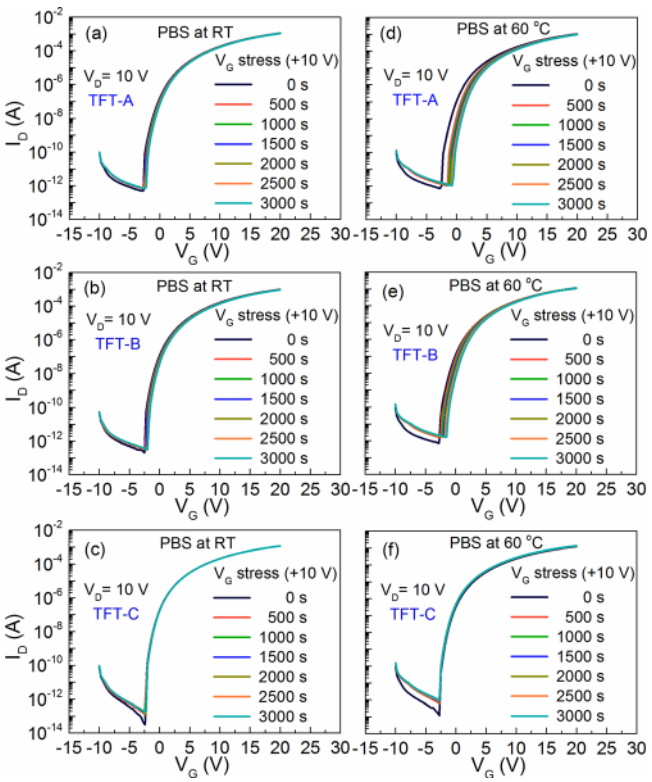

FIG. 2. Transfer curves of (a) TFT-A, (b) TFT-B, and (c) TFT-C measured under different durations of PBS at RT. Transfer curves of (d) TFT-A, (e) TFT-B, and (f) TFT-C measured under different durations of PBS at 60 °C.

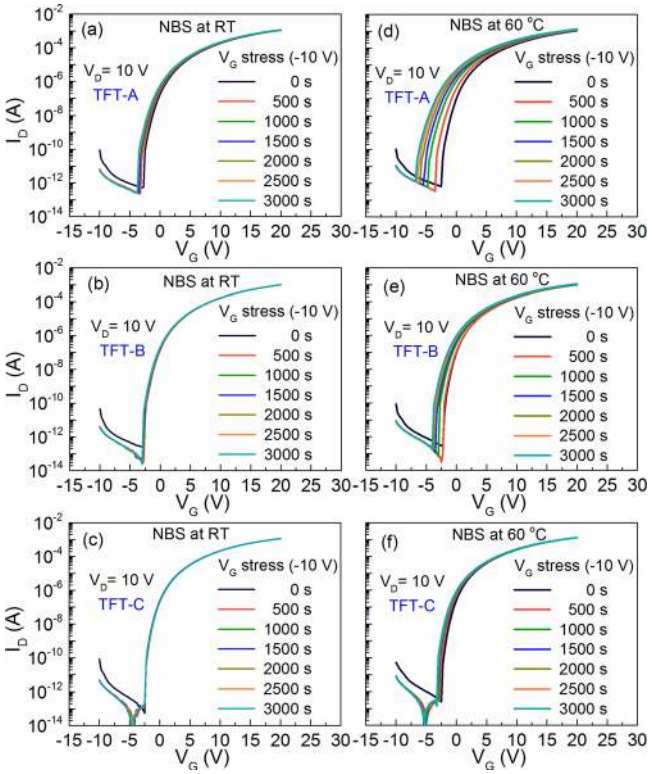

FIG. 3. Transfer curves of (a) TFT-A, (b) TFT-B, and (c) TFT-C measured under different durations of NBS at RT. Transfer curves of (d) TFT-A, (e) TFT-B, and (f) TFT-C measured under different durations of NBS at 60 °C.

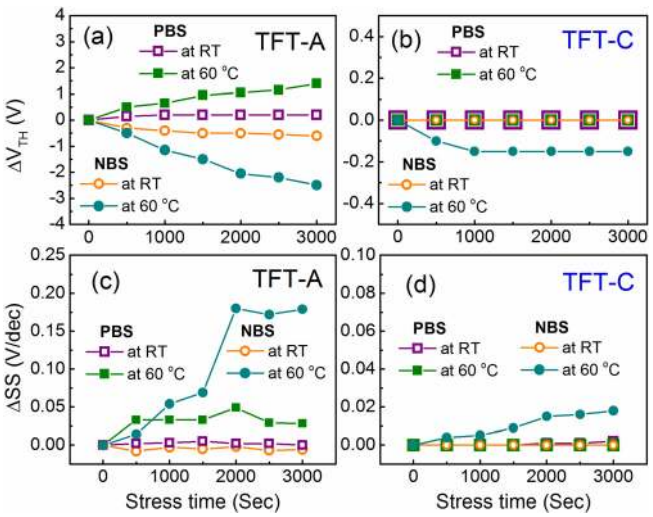

FIG. 4. Time dependent ΔV_{TH} shift due to PBS and NBS measured at RT and 60 °C for (a) TFT-A and (b) TFT-C. Time dependent ΔSS change due to PBS and NBS measured at RT and 60 °C for (c) TFT-A and (d) TFT-C.

significant change in ΔV_{TH} (Fig. 4(b)) and ΔSS (Fig. 4(d)). Under NBS at 60 °C (Fig. 3(f)), TFT-C exhibited a very low ΔV_{TH} of −0.15 V (Fig. 4(c)), which is much less than the V_{TH} shift of TFT-A ($\Delta V_{TH} = -2.5$ V) and TFT-B ($\Delta V_{TH} = -1.2$ V). The ΔSS in case of TFT-C under NBS at 60 °C (0.017 V/dec) is much less than the ΔSS value of the TFT-A (0.178 V/dec). It may be noted that we have also fabricated a device with a very similar structure to that of TFT-B but having about 3 times thicker HfO_2 layer on top of the ZnO layer. However, this device resulted about 30% lower mobility compared to other TFTs and it also showed a similar trend of gate bias stress instability as observed in case of TFT-B (results are not shown here).

Material characterization of the channel layers was performed to understand the role of HfO_2 layers on PBS and NBS stabilities. Figs. 5(a) and 5(b) show the cross-sectional aberration corrected high-angle annular dark-field scanning transmission electron microscopy (HAADF-STEM) image of single layer ZnO and ZnO/HfO_2 multilayer along with the ITO (gate) and HfO_2 (dielectric) as used in TFT-A and TFT-C, respectively. The average thickness of the single layer ZnO film in TFT-A was found to be 22.3 ± 1.2 nm. Three layers of ZnO embedded between the gate dielectric and three thin HfO_2 layers can be clearly seen from Fig. 5(b). The average thickness of the ZnO and HfO_2 layers in TFT-C were found to be 7.2 ± 0.7 nm and 1.2 ± 0.3 nm, respectively. In both cases, ZnO and HfO_2 were found to be poly-crystalline and amorphous, respectively. The inset of Fig. 5(b) shows the HAADF-STEM energy dispersive spectroscopy (EDS) line profile of Hf and Zn obtained from the region as indicated by the white arrow. Both HAADF-STEM image and the EDS line profile clearly show the expected signal variation of Hf and Zn and suggest that the HfO_2 layers largely remains as a separate layer, although any diffusion of Hf into ZnO or Zn into HfO_2 layer cannot be ruled out, which is beyond the detection limit of the instrument used.

X-ray photoelectron spectroscopy (XPS) O1s spectra of the channel layers used in TFT-A and TFT-C are shown in Figs. 6(a) and 6(b), respectively. In both cases, the Gaussian fitting of the O1s peak exhibited a strong peak at 529.9 eV along with two shoulder peaks at ~530.9 eV and ~532.0 eV.

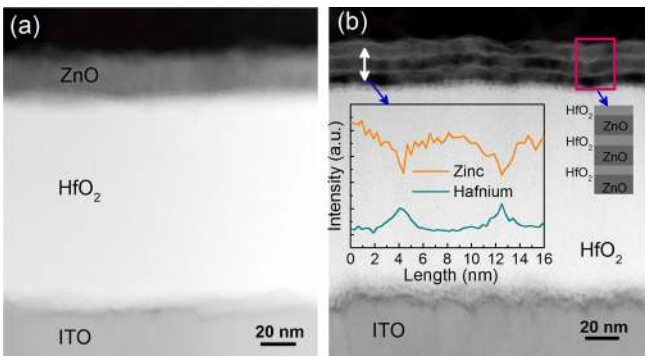

FIG. 5. Cross-sectional HAADF-STEM image of (a) single layer ZnO and (b) ZnO/HfO_2 multilayer structure channel layer as used in TFT-A and TFT-C, respectively. The left side inset to (b) shows the EDS line profile of Hf and Zn of the corresponding film. The right side inset to (b) shows the schematic representation of the ZnO/HfO_2 multilayer structure.

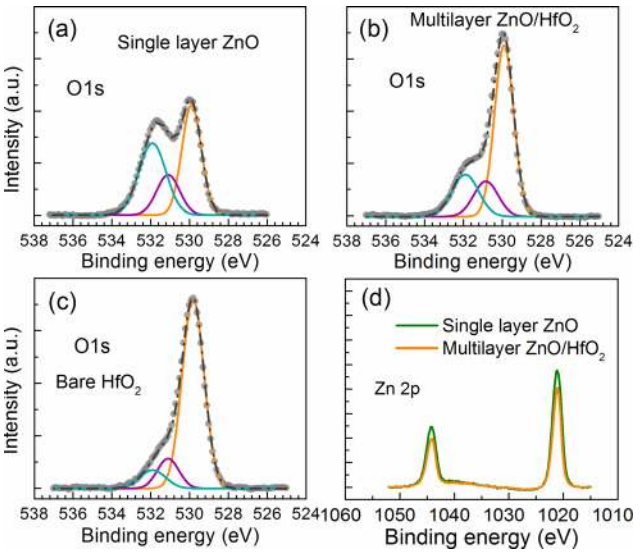

FIG. 6. XPS O1s spectra of the (a) single layer ZnO and (b) ZnO/HfO_2 multilayer channel as used in TFT-A and TFT-C, respectively. (c) XPS O1s spectra of a bare HfO_2 film and (d) XPS Zn2p spectra of the single layer ZnO and ZnO/HfO_2 multilayer films.

The peak at 529.9 eV is attributed to the oxygen in ZnO lattice without oxygen vacancy (O_L) and the peaks at ~530.9 and ~532.0 eV are attributed to the oxygen in ZnO lattice with oxygen vacancy (O_V) and the OH groups attached to zinc ions (O_H), respectively.[16] Fig. 6(c) shows the XPS O1s spectra of a bare HfO_2 film as reference, which also exhibited similar O1s peaks approximately at the same binding energies as observed in case of ZnO film. It is clearly seen that a large number of OH-groups [$O_H/(O_L + O_V + O_H) = 38.9\%$] are present in case of TFT-A channel layer compared to the TFT-C channel layer [$O_H/(O_L + O_V + O_H) = 21.1\%$]. The OH concentration [$O_H/(O_L + O_V + O_H) = 8\%$] in case of bare HfO_2 film was found to be much lower than the TFT-A and TFT-C channel layers. It may be noted here that the channel layer used in case of TFT-B also showed a similar amount of OH concentration (results are not shown here). Fig. 6(d) shows the XPS Zn2p spectra of TFT-A and TFT-C channel layers. Intensity of the Zn2p peaks in case of TFT-C channel layer is slightly lower than that of the TFT-A channel layer, which may be attributed to the total penetration depth of X-ray into the ZnO layer due to the presence of thin HfO_2 layer on the top of the ZnO layer.

The shifting of V_{TH} without significant change in SS has been attributed to the charge trapping in the dielectric and/or at the dielectric/semiconductor interface.[11,18] As HfO_2 was used as the dielectric in all the TFTs, thus charge trapping in the dielectric can be neglected. It has been reported that adsorbed oxygen and water molecules at the back channel plays an important role in the stability of un-passivated oxide TFTs.[19] It is believed that adsorbed oxygen molecules can act as acceptor-like states and hence cause positive V_{TH} shift.[20,21] Similarly, adsorbed water molecules have been reported to act as donor-like surface states,[22] which causes negative ΔV_{TH} shift.[13] However, Kim *et al.*[23] have reported that water molecules can act as an electron trap and/or donor, depending on the amount of water adsorbed on the back-channel surface. Recently, Zhang *et al.* have reported that

water assisted oxygen absorption lead to a significant V_{TH} shift under PBS.[24] Further, it is believed that the adsorbed water molecules at the back channel can diffuse towards the channel/gate dielectric interface,[25] generating a large number of metastable gap states leading to a large number of trapped electrons and eventual increase in hole carrier density, and thus exhibiting larger negative ΔV_{TH} under NBS.[13] The adsorbed oxygen concentration is believed to decrease at higher temperature leading to an increase in doubly charged oxygen vacancies (V_O^{2+}) in the ZnO layer.[15] The ionized V_O^{2+} charges would be accumulated at the channel/gate dielectric interface upon the application of NBS and hence exhibits a large negative V_{TH} shift.[16] This assumption is well consistent with the increased ΔSS value of TFT-A and TFT-C under NBS at 60 °C, as shown in Figs. 4(c) and 4(d), suggesting the creation of defect states at the channel/gate dielectric interface or in the channel layer.

From our XPS results, it is found that TFT-A channel layer (Fig. 6(a)) has significantly large number of OH-groups compared to the TFT-C channel layer (Fig. 6(b)). Due to its polycrystalline nature, ZnO can have many grain boundaries where a large number of adsorbed water molecules can move easily towards the ZnO channel/dielectric layer interface, in case of TFT-A. Thus, considering the bias stability results available in the literature as mentioned above, it can be inferred that the adsorbed water molecules are the main cause of threshold voltage instability. The bias stability could be improved using one layer of HfO_2 on top of ZnO layer as used in case of TFT-B. The HfO_2 acts as a passivation layer, which prevents the adsorption of water or oxygen molecules into the ZnO layer and hence improves the bias stability.[15,23,26] It is also noted that a single HfO_2 layer in the middle of two ZnO layers showed very similar trend of bias stress instability to that of TFT-A (results not shown here). Thus, a single HfO_2 layer at the top or in the middle of ZnO layer is not sufficient to effectively prevent the diffusion of water molecules toward the channel/dielectric layer interface. However, we believe that in case of the TFT-C, the water molecules adsorbed at the back channel may have to travel non-linear (longer) paths through the multiple layers of amorphous HfO_2, which should have significantly less number of adsorption sites. Further, due to the presence of multiple layers of HfO_2 at different depths, the diffusion time of the water molecules can be significantly increased and hence the number of water molecules reaching the semiconductor/dielectric interface is effectively minimized. The HfO_2 multilayers also possibly prevent the movement of ionized V_O^{2+} charges from the bulk towards the channel/gate dielectric interface, and hence concurrently improve the NBS stability even at higher temperature.

In summary, we have developed a ZnO/HfO_2 multilayer structure semiconducting channel layer to improve the gate-bias stress stability of ZnO TFTs. TFTs with very stable performance could be obtained using multiple layers of ZnO embedded between HfO_2 layers as the channel layer. The developed multilayer structure channel layer can potentially be used for display and other electronic applications.

Research reported in this publication was supported by King Abdullah University of Science and Technology (KAUST).

[1]E. Fortunato, P. Barquinha, and R. Martins, Adv. Mater. **24**, 2945 (2012).
[2]J. Y. Kim, S. Noh, D. Lee, P. K. Nayak, Y. Hong, and C. Lee, J. Nanosci. Nanotechnol. **11**, 5995 (2011).
[3]P. K. Nayak, J. Yang, J. Kim, S. Chung, J. Jeong, C. Lee, and Y. Hong, J. Phys. D: Appl. Phys. **42**, 035102 (2009).
[4]P. K. Nayak, J. A. Caraveo-Frescas, U. S. Bhansali, and H. N. Alshareef, Appl. Phys. Lett. **100**, 253507 (2012).
[5]E. M. C. Fortunato, P. M. C. Barquinha, A. C. M. B. G. Pimentel, A. M. F. Goncalves, A. J. S. Marques, L. M. N. Pereira, and R. F. P. Martins, Adv. Mater. **17**, 590 (2005).
[6]P. K. Nayak, J. Jang, C. Lee, and Y. Hong, Appl. Phys. Lett. **95**, 193503 (2009).
[7]R. L. Hoffman, B. J. Norris, and J. F. Wager, Appl. Phys. Lett. **82**, 733 (2003).
[8]J. Siddiqui, E. Cagin, D. Chen, and J. D. Phillips, Appl. Phys. Lett. **88**, 212903 (2006).
[9]D. L. Zhao, D. A. Mourey, and T. N. Jackson, J. Electron. Mater. **39**, 554 (2010).
[10]N. Huby, S. Ferrari, E. Guziewicz, M. Godlewski, and V. Osinniy, Appl. Phys. Lett. **92**, 023502 (2008).
[11]R. B. M. Cross and M. M. De Souza, Appl. Phys. Lett. **89**, 263513 (2006).
[12]P. K. Nayak, J. V. Pinto, G. Goncalves, R. Martins, and E. Fortunato, J. Disp. Technol. **7**, 640 (2011).
[13]K. H. Lee, J. S. Jung, K. S. Son, J. S. Park, T. S. Kim, R. Choi, J. K. Jeong, J. Y. Kwon, B. Koo, and S. Lee, Appl. Phys. Lett. **95**, 232106 (2009).
[14]J. M. Lee, I. T. Cho, J. H. Lee, and H. I. Kwon, Appl. Phys. Lett. **93**, 093504 (2008).
[15]S. Yang, D. H. Cho, M. K. Ryu, S. H. K. Park, C. S. Hwang, J. Jang, and J. K. Jeong, IEEE Electron Device Lett. **31**, 144 (2010).
[16]B. S. Yang, M. S. Huh, S. Oh, U. S. Lee, Y. J. Kim, M. S. Oh, J. K. Jeong, C. S. Hwang, and H. J. Kim, Appl. Phys. Lett. **98**, 122110 (2011).
[17]Y. S. Rim, D. L. Kim, W. H. Jeong, and H. J. Kim, Electrochem. Solid-State Lett. **15**, H37 (2012).
[18]J. J. Siddiqui, J. D. Phillips, K. Leedy, and B. Bayraktaroglu, IEEE Trans. Electron Devices **59**, 1488 (2012).
[19]J. F. Conley, IEEE Trans. Device Mater. Reliab. **10**, 460 (2010).
[20]J. K. Jeong, H. W. Yang, J. H. Jeong, Y. G. Mo, and H. D. Kim, Appl. Phys. Lett. **93**, 123508 (2008).
[21]D. Kang, H. Lim, C. Kim, I. Song, J. Park, Y. Park, and J. Chung, Appl. Phys. Lett. **90**, 192101 (2007).
[22]J. S. Park, J. K. Jeong, H. J. Chung, Y. G. Mo, and H. D. Kim, Appl. Phys. Lett. **92**, 072104 (2008).
[23]D. Kim, S. Yoon, Y. Jeong, Y. Kim, B. Kim, and M. Hong, Appl. Phys. Express **5**, 021101 (2012).
[24]J. Zhang, X. F. Li, J. G. Lu, N. J. Zhou, P. J. Guo, B. Lu, X. H. Pan, L. Chen, and Z. Z. Ye, RSC Adv. **4**, 3145 (2014).
[25]M. E. Lopes, H. L. Gomes, M. C. R. Medeiros, P. Barquinha, L. Pereira, E. Fortunato, R. Martins, and I. Ferreira, Appl. Phys. Lett. **95**, 063502 (2009).
[26]A. Olziersky, P. Barquinha, A. Vila, L. Pereira, G. Goncalves, E. Fortunato, R. Martins, and J. R. Morante, J. Appl. Phys. **108**, 064505 (2010).